JACS
JOURNAL OF THE AMERICAN CHEMICAL SOCIETY
Article
pubs.acs.org/JACS

Synthesis of Silylene-Bridged Endohedral Metallofullerene $Lu_3N@I_h$-C_{80}

Kumiko Sato,[†] Masahiro Kako,[‡] Mitsuaki Suzuki,[†] Naomi Mizorogi,[†] Takahiro Tsuchiya,[†] Marilyn M. Olmstead,[§] Alan L. Balch,[§] Takeshi Akasaka,*[,†] and Shigeru Nagase[∥]

[†]Life Science Center of Tsukuba Advanced Research Alliance, University of Tsukuba, Ibaraki 305-8577, Japan
[‡]Department of Engineering Science, The University of Electro-Communications, Chofu 182-8585, Japan
[§]Department of Chemistry, University of California, Davis, California 95616, United States
[∥]Fukui Institute for Fundamental Chemistry, Kyoto University, Kyoto 606-8103, Japan

Supporting Information

ABSTRACT: Functionalization of endohedral metallofullerenes has been shown to differ depending on photochemical or thermal pathways. We report that $Lu_3N@I_h$-C_{80} reacts with thermally generated bis(2,6-diethylphenyl)silylene with high selectivity and forms monosilylated derivative **1b**. Unexpectedly, **1b** undergoes photochemical conversion to afford isomer **1a** under ambient light. These adducts were characterized using NMR, visible−near-IR spectroscopy, and matrix-assisted laser desorption ionization time-of-flight mass spectrometry. Single-crystal X-ray structure determination of **1a** reveals a rare example of an open 1,2-adduct at the [5,6]-ring junction of the I_h-C_{80} cage. The electrochemical study reveals that the redox potentials of **1a** and **1b** are shifted cathodically compared to those of pristine $Lu_3N@I_h$-C_{80} and that monosilylation is effective to fine-tune the electronic properties of endohedral metallofullerenes as well as empty fullerenes. Density functional theory calculations were also performed, which provide a theoretical basis for the structures and the behavior of the encapsulated Lu_3N cluster.

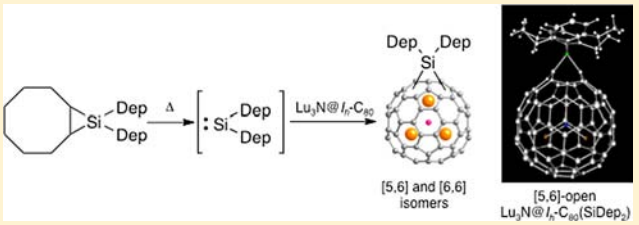

INTRODUCTION

Many research groups have investigated the chemical reactivity of endohedral metallofullerenes (EMFs), the properties of which have been proven to differ greatly from those of empty fullerenes.[1] The electronic structures of EMFs are of great interest because the encaged metal atoms and the carbon cages are regarded to have cationic and anionic characters, respectively, as a result of electron transfer. After many years of study, exohedral chemical functionalization[1b−e] is widely recognized as an effective method for modifying the physical and chemical properties of EMFs, which can serve as functional materials in molecular electronics, nanomaterials sciences,[2] and biochemistry.[3]

To design new valuable organofullerenes for these applications, it is necessary to understand how exohedral chemical functionalization affects the electronic properties of fullerenes. Introduction of heteroatoms such as electropositive silicon directly onto fullerene surfaces has induced remarkable changes in the electronic characteristics of fullerenes.[4] We have described the derivatization of EMFs by the addition of reactive silicon compounds, such as disiliranes[5] and siliranes.[6] In fact, electrochemical analysis and theoretical calculation revealed that silylated fullerene derivatives have more negative charge on the cage than the parent fullerenes have. Moreover, we have demonstrated that the number of silicon atoms on the fullerene surface plays an important role in the electronic properties and the movement of the encapsulated metal atoms. For example, the three-dimensional movement of metal atoms in $M_2@I_h$-C_{80} is restricted to two-dimensional movement because silylation alters the electrostatic potentials and thereby the dynamic behavior of the cationic metals.[5a−c] Such regulation of the dynamic behavior of the encaged species will be useful for the application of EMFs as functional materials in molecular electronics. Nevertheless, silylation of EMFs has been hitherto limited to bis-silylation[5] and carbosilylation[6] using disiliranes and siliranes. Therefore, it is valuable to develop convenient and versatile synthetic methods for silylation to provide various silylated EMFs. As a candidate for monosilylating reagents for EMFs, silylenes, divalent silicon species, are promising compounds because the addition of silylenes to unsaturated C−C bonds occurs readily.[7] Carbenes, the carbon analogues of silylenes, are well-known as common reagents for exohedral functionalization of EMFs[1,8] and hollow fullerenes.[9] In fact, photochemically generated silylenes react with C_{60} and C_{70} to afford the corresponding silylene adducts.[10]

In this paper we describe the monosilylation of $Lu_3N@I_h$-C_{80},[11] which is widely known as a trimetallic nitride templated (TNT) endohedral metallofullerene. To achieve effective silylation, we used a new silylene precursor, 9,9-bis(2,6-

Received: July 27, 2012
Published: September 4, 2012

   dx.doi.org/10.1021/ja3073929 | J. Am. Chem. Soc. 2012, 134, 16033−16039

diethylphenyl)-9-silabicyclo[6.1.0]nonane (**2**), which can generate silylene efficiently under both thermal and photochemical conditions (Scheme 1). Additionally described is the detailed

Scheme 1

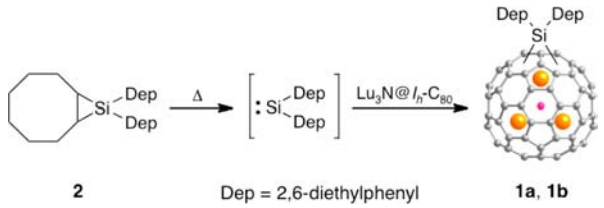

characterization of two obtained products corresponding to $Lu_3N@I_h$-C_{80}(SiDep$_2$). Of particular interest is the isolation of a silylene-bridged silafulleroid structure, which represents a rare example of an open type of 1,2-adduct at the [5,6]-ring junction of the I_h-C_{80} cage. To the best of our knowledge, the only other example is a recent report of azide addition to $Sc_3N@I_h$-C_{80} to form a [5,6] azafulleroid.[8g]

RESULTS AND DISCUSSION

Synthesis of $Lu_3N@I_h$-C_{80}(SiDep$_2$) 1a and 1b. The reaction of $Lu_3N@I_h$-C_{80} with the silylene precursor **2** (see the Supporting Information) was conducted as follows (Scheme 1). A solution of $Lu_3N@I_h$-C_{80} (2.0 mg, 1.3×10^{-6} mol) and **2** (13.7 mg, 3.4×10^{-5} mol) in 1,2-dichlorobenzene (ODCB; 20 mL) was placed in a Pyrex tube and degassed using freeze–pump–thaw cycles under reduced pressure. It was then heated for 23 min at 180 °C under an argon atmosphere in the dark. After the solution was cooled, a small portion of the solution was analyzed by high-performance liquid chromatography (HPLC) using a Buckyprep column. The HPLC chromatogram revealed a new fraction (peak F_1) corresponding to a product with high intensity (Figure 1). In addition, another fraction

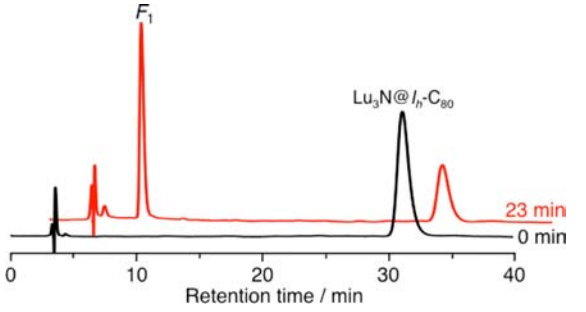

Figure 1. HPLC profiles of the crude reaction mixture. Conditions: Buckyprep column (⌀ = 4.6 × 250 mm); eluent, toluene; flow rate, 1.0 mL/min; wavelength, 330 nm; room temperature.

(F_2) appeared at a slightly earlier retention time which gradually increased when the reaction mixture was exposed to ambient light at room temperature, as shown in Figure 2.

Subsequently, the reaction mixture was separated by preparative HPLC using a Buckyprep and a 5NPE column. Two compounds, **1a** and **1b**, were obtained from HPLC fractions F_2 and F_1 (Figure S1; see the Supporting Information). Additional analysis of **1a** and **1b** using matrix-assisted laser desorption ionization time-of-flight (MALDI-TOF) mass spectrometry showed weak peaks at m/z 1793, which correspond to the molecular ion peak for the isomeric

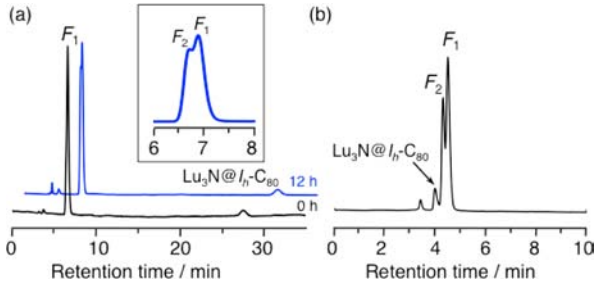

Figure 2. (a) HPLC profiles of the reaction mixture exposed to ambient light. Conditions: Buckyprep column (⌀ = 4.6 × 250 mm); eluent, toluene; flow rate, 1.0 mL/min; wavelength, 330 nm; room temperature. (b) HPLC profile of the reaction mixture exposed to ambient light for 12 h. Conditions: 5NPE column (⌀ = 4.6 × 250 mm); eluent, toluene; flow rate, 1.0 mL/min; wavelength, 330 nm; room temperature.

silylene adduct $Lu_3N@I_h$-C_{80}(SiDep$_2$) (see the Supporting Information, Figure S2). In addition, strong fragment peaks were observed at m/z 1499 for **1a** and **1b**, which are assignable to the parent cage, $Lu_3N@I_h$-C_{80}. Therefore, it is reasonable to assume that the silylene Dep$_2$Si, generated by the thermal extrusion from **2**, reacted with $Lu_3N@I_h$-C_{80} to afford **1b**, which isomerized slowly to **1a** under room light. It is noteworthy that multiadducts such as $Lu_3N@I_h$-C_{80}(SiDep$_2$)$_2$ were not observed. Consequently, silylation using **2** produces selective derivatization of $Lu_3N@I_h$-C_{80}. It is further confirmed that exposure of a degassed ODCB solution of **1b** to ambient light afforded **1a** and pristine $Lu_3N@I_h$-C_{80} within 24 h (Figure 3a).

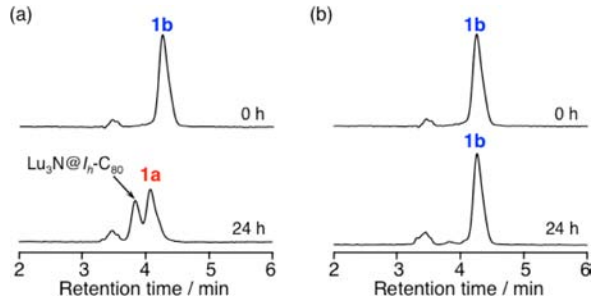

Figure 3. HPLC monitoring of a solution of **1b** in ODCB under degassed conditions at room temperature (a) in the presence of ambient light and (b) in the absence of ambient light. Conditions: 5NPE column (⌀ = 4.6 × 250 mm); eluent, toluene; flow rate, 1.0 mL/min; wavelength, 330 nm; room temperature.

Under the same conditions, **1a** in ODCB decomposed to give $Lu_3N@I_h$-C_{80} (Figure 4a). Although **1a** and **1b** are photolabile, both isomers are stable in the dark at room temperature (Figures 3b and 4b).

Although **2** efficiently generates the silylene Dep$_2$Si by irradiation using a medium-pressure mercury lamp, UV irradiation of an ODCB solution of **2** and $Lu_3N@I_h$-C_{80} gave neither **1a** nor **1b**, while starting materials were consumed. The co-photolysis of $Lu_3N@I_h$-C_{80} and **2** is expected to be disadvantageous for the synthesis of **1a** and **1b** because these adducts degrade to eliminate the silylene addend by photoirradiation, as described above.

For comparison, we examined the reaction of $Sc_3N@I_h$-C_{80},[1e] which is the most abundant and well-explored TNT EMF, with Dep$_2$Si. However, the addition reactions of $Sc_3N@I_h$-C_{80} and Dep$_2$Si proceeded much less efficiently to afford poor yields of

dx.doi.org/10.1021/ja3073929 | J. Am. Chem. Soc. 2012, 134, 16033–16039

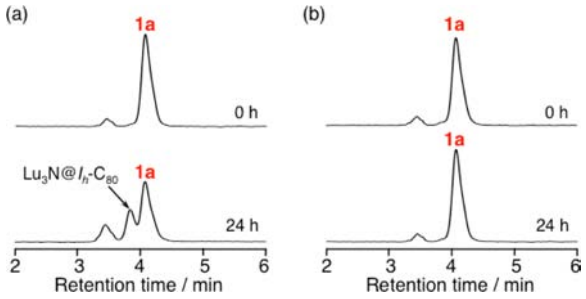

Figure 4. HPLC monitoring of a solution of **1a** in ODCB under degassed conditions at room temperature (a) in the presence of ambient light and (b) in the absence of ambient light. Conditions: 5NPE column (⌀ = 4.6 × 250 mm); eluent, toluene; flow rate, 1.0 mL/min; wavelength, 330 nm; room temperature.

adducts under thermal or photochemical conditions that are identical with those for $Lu_3N@I_h$-C_{80}. The isolation and structural analyses were frustrated because of low quantities of the adducts, which were confirmed only by MALDI-TOF mass spectrometry. Recently, Echegoyen et al. reported the reactions of electrochemically generated $M_3N@I_h$-C_{80} dianions (M = Sc, Lu) with electrophiles and ascribed the superior reactivity of $Lu_3N@I_h$-C_{80} dianion according to the localization of its highest occupied molecular orbital (HOMO) on the cage.[13c] Although the origin of the different reactivities of $M_3N@I_h$-C_{80} toward Dep_2Si has not been clarified at present, the HOMOs of $M_3N@I_h$-C_{80} may play an important role in the reactions with silylenes, weak electrophiles. We are currently investigating the reactivities of $M_3N@I_h$-C_{80} with several organosilicon compounds.

Structural Determination of 1a and 1b. For the structural characterization of **1a** and **1b**, NMR analysis and X-ray crystallography were performed. There are four possible isomeric structures for the derivatized I_h-C_{80} cage resulting

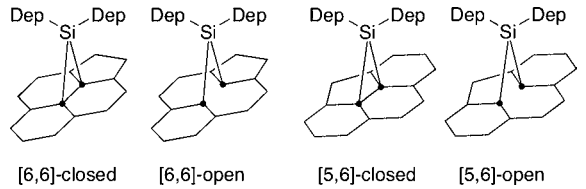

Figure 5. Addition patterns of $Lu_3N@I_h$-$C_{80}(SiDep_2)$.

from 1,2-addition of a silylene bridge as shown in Figure 5. The ^{1}H NMR spectra of **1a** and **1b** are shown in Figure S3 (see the Supporting Information). The addition of Dep_2Si at the [5,6]-ring junction will make the two Dep substituents nonequivalent, whereas addition at the [6,6]-ring junction will produce equivalent Dep moieties. Therefore, we specifically examined the ^{1}H NMR signals of the aryl *para* protons of the Dep rings. The spectrum of **1a** displays a pair of triplets at 7.47 and 7.42 ppm, which are assigned as nonequivalent aryl *para* protons, and suggests that the Dep_2Si group is bridged over the [5,6]-ring junction (Figure S3a, Supporting Information). In contrast, the spectrum of **1b** exhibits one triplet signal at 7.50 ppm, which reflects the equivalency of the two Dep groups (Figure S3b). These observations suggest that **1a** and **1b** are Dep_2Si adducts at the [5,6]-ring and [6,6]-ring junctions, respectively. ^{13}C NMR measurements can help to establish whether these compounds are silacyclopropane derivatives or open cage silafulleroids. The ^{13}C NMR spectrum of **1a** showed 44 signals from the sp^2 carbon atoms of the I_h-C_{80} cage, as well as four quaternary sp^2 carbons of the Dep groups between 70 and 155 ppm (Figure S4; see the Supporting Information). In addition, four tertiary sp^2 carbons and two sets of ethyl carbons of the nonequivalent Dep groups were observed, which is consistent with ^{1}H NMR results described above. These spectral data suggest that **1a** has C_s symmetry, resulting from 1,2-addition of Dep_2Si at the [5,6]-ring junction of the I_h-C_{80} cage. Consequently, the structure of **1a** is determined to be the silylene-bridged silafulleroid type, which represents the rare example of an [5,6]-open I_h-C_{80} EMF derivative. However, the ^{13}C NMR spectrum of **1b** showed two nonequivalent singlet signals at 85.14 and 77.17 ppm, which are ascribed to the sp^3 carbons of the silacyclopropane ring (Figure S5 in the Supporting Information). Previously, we reported the synthesis of the fullerene−silylene adducts $C_{60}SiDip_2$[10a] and $C_{70}SiDip_2$[10b] (Dip = 2,6-diisopropylphenyl) with silacyclopropane structures. The sp^3 carbon signals of the silacyclopropane rings were observed at 71.12 ppm for $C_{60}SiDip_2$ and 78.51 and 67.77 ppm for $C_{70}SiDip_2$. In the ^{13}C NMR spectrum of **1b**, 45 sp^2 carbon signals are assigned to 42 carbons of the I_h-C_{80} cage and 3 quaternary aromatic carbons of the Dep groups. As for the tertiary sp^2 ring carbons of the Dep groups, one signal for the *para*-position and two signals for the *meta*-positions are observed. Four additional sp^3 carbon signals are also found for the two sets of ethyl groups in the upfield region. The lowered spectral symmetry of the Dep groups is rationalized on the basis of restriction of the free rotation of the two equivalent Dep rings in **1b** as a result of steric constraints. These observations are consistent with the structure of **1b** with C_s symmetry. Therefore, it is concluded that **1b** should be a "closed" silamethanofullerene rather than a silafulleroid (Figure S3b).

Visible−near-infrared (vis−NIR) spectroscopy is a useful method for characterization of the electronic structures of hollow fullerenes and EMFs. Moreover, exohedrally functionalized fullerenes show characteristic vis−NIR spectra that are more dependent on the regiochemistry of functionalization than on the type of functional group.[6,8,11,15,16] For example, the spectra of 1,4-$Sc_3N@I_h$-$C_{80}(Mes_2Si)_2CH_2$[5b] and 1,4-$Sc_3N@I_h$-$C_{80}(CH_2C_6H_5)_2$[12] are quite similar, with absorption maxima around 900 nm, although they have different substituents. The vis−NIR absorption spectra of **1a** and **1b** are shown with that of $Lu_3N@I_h$-C_{80} in Figure 6. The spectrum of **1b** shows a distinctive absorption maximum around 700 nm, which resembles those of the reported [6,6]-methano-bridged $Lu_3N@I_h$-C_{80} derivatives.[13] This spectral similarity supports the assignment of **1b** as the [6,6]-adduct, as determined by ^{1}H and ^{13}C NMR analyses. Meanwhile, **1a** shows a broad and gently sloping absorption around 700 nm with no characteristic absorption maximum. This finding also confirmed that vis−NIR spectra of derivatized isomers of EMFs are specific to the regiochemistry of derivatization. It is worth noting that the spectrum of **1a** shows no resemblance to that of 1,4-$Lu_3N@I_h$-$C_{80}(CH_2C_6H_5)_2$, which was reported to have a noticeable absorption maximum around 800 nm.[12]

Fortunately, a thin red crystal suitable for X-ray diffraction was obtained from a solution of **1a** in a mixture of CS_2/ODCB at 0 °C with the addition of hexane to lower the solubility of the adduct. The structure of **1a** was determined by X-ray structural analysis. A drawing of the adduct is shown in Figure S6 (see the Supporting Information), with selected bond

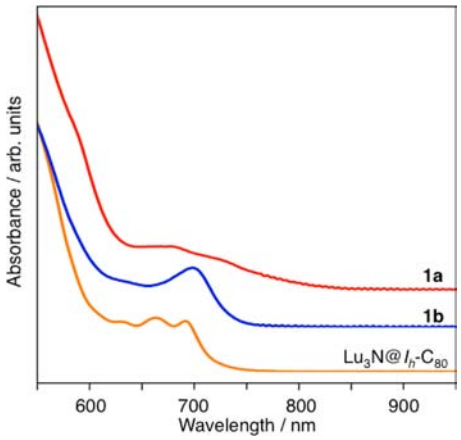

Figure 6. Vis−NIR absorption spectra of **1a**, **1b**, and $Lu_3N@I_h$-C_{80}.

lengths in Table S1. The crystal structure of **1a** shows some disorder in the positions of both the Lu_3N cluster and the cage carbon atoms. There are two orientations of the C_{80} cage that have a pseudo-D_{5d} symmetry of the derivatized I_h-C_{80}. These cages are related by a crystallographic mirror plane and occupy a common site. Such disorder is frequently observed when addition occurs at [5,6] ring junctions.[15b]

Only one of these orientations and the primary Lu_3N unit, which consists of N1, Lu1, Lu3, and Lu3′ (symmetry code′ 1/2 − *x*, 1/2 − *y*, *z*), are shown in Figure S7, Supporting Information. Lu1 is situated on the crystallographic mirror plane with a fractional occupancy of 0.96. Lu3 and Lu3′ have fractional occupancies of 0.85. Lu3′ is generated by reflection of Lu3 through a crystallographic mirror plane.

The X-ray structure showed unambiguously that the addition of silylene to the I_h-C_{80} cage had occurred at the [5,6]-ring junction. In addition, the C1−C2 distance at the site of silylene functionalization elongated to 2.25(5) Å, which confirms that **1a** possesses an open structure. The open structure with aza-bridged (4-isopropoxyphenyl)nitrene at the [5,6] position of $Sc_3N@I_h$-C_{80} yielded a C1−C2 distance of 2.161(2) Å, in general agreement with the shorter covalent radius of N relative to Si.[8g] Open structures at [6,6]-ring junctions on the I_h-C_{80} cage have been reported for $La_2@I_h$-C_{80}(Ad) and $Y_3N@I_h$-$C_{80}C(CO_2CH_2Ph)_2$, for which the functionalized C−C distances are 2.164(3) and 2.30(3) Å, respectively.[8e,14a] The distance of the C1−C2 separation at the [5,6]-ring junction in **1a** is nearly as long as those of the functionalized [5,6]- and [6,6]-ring junctions. The Si−C bond lengths (Si1−C1, 1.87(3) Å; Si1−C2, 1.88(3) Å) between the addend and the I_h-C_{80} cage are close to the normal Si−C single bond lengths in organosilanes.

The encapsulated Lu_3N cluster shows disorder of the Lu atoms, whereas the N atom has one site, which lies on a crystallographic mirror plane. The primary Lu_3N unit is planar, with the sum of Lu−N−Lu bond angles being 360.0° (Lu1−N1−Lu3, 120.3(7)°; Lu1−N1−Lu3′, 120.3(7)°; Lu3−N1−Lu3′, 119.4(7)°). The Lu−N bond lengths (Lu1−N1, 2.03(1) Å; Lu3−N1, 2.096(7) Å; Lu3′−N1, 2.096(7) Å) are comparable to those reported for pristine $Lu_3N@I_h$-C_{80}, which range from 1.980(6) to 2.0819(8) Å (Table S1, Supporting Information).[11] The Lu1 atom points to the silylated site and is almost collinear with the N1 and Si1 atoms, as indicated by the N1−Lu1−Si1 bond angle (180.0(4)°).

The positional relation between the cage and Lu atoms was also investigated. As shown in Figure 7, Lu3 and Lu3′ reside

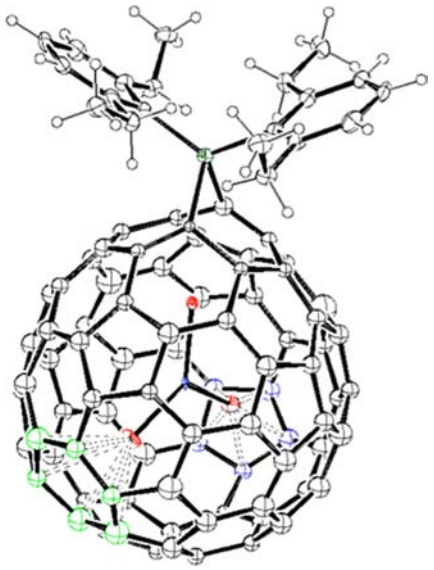

Figure 7. Relation between cage and Lu atoms in **1a**: Lu, red; N, blue, Si, green; C closest to Lu3, yellow-green; C closest to Lu3′, purple.

close to a hexagon and a pentagon highlighted respectively in yellow-green and purple in the interior of the cage. The distances from Lu3 to the nearest carbon atoms of the cage range from 2.37(3) to 2.47(3) Å, whereas those from Lu3′ fall within a range from 2.23(3) to 2.56(3) Å. In addition, the distances between Lu1 and C1 and C2, the [5,6]-ring carbons functionalized by silylene, are 2.54(3) and 2.53(3) Å, respectively. These nonbonded Lu−C distances are slightly elongated compared to those of pristine $Lu_3N@I_h$-C_{80} (2.112(7)−2.220(7) Å),[11] as a result of the addition of the silylene. The orientation of the Lu_3N cluster, in which one Lu atom points to the functionalized site, is similar to those of the methanofulleroid derivatives of $M_3N@I_h$-C_{80} (M = Sc, Y).[14]

Electrochemical Properties of 1a and 1b. The redox potentials of **1a** and **1b** were measured using cyclic voltammetry (CV) and differential pulse voltammetry (DPV) and are listed in Table 1 along with those of related compounds. The voltammograms of **1a** and **1b** are presented

Table 1. Redox Potentials (V)[a] of 1a, 1b, $Lu_3N@I_h$-C_{80}, and Silylated EMFs

compd	E^{ox}_1	E^{red}_1	E^{red}_2	E^{red}_3
$Lu_3N@I_h$-C_{80}	+0.61	−1.39[b]	−1.83[b]	−2.16[b]
1a	+0.27[b]	−1.43[b]	−1.72[b]	−1.94[b]
1b	+0.43[b]	−1.52[b]	−1.73[b]	−1.99[b]
$Sc_3N@I_h$-C_{80}[c]	+0.62	−1.22		
$Sc_3N@I_h$-$C_{80}(Mes_2Si)_2CH_2$[c]	+0.08[b]	−1.45		
$La_2@I_h$-C_{80}[d]	+0.56	−0.31	−1.71	−2.13
$La_2@I_h$-$C_{80}(Dep_2Si)_2CH_2$[e]	−0.04[b]	−0.70		
$La_2@I_h$-$C_{80}(Dep_2Si)CH_2CH$(*t*-BuPh)-2A[f]	+0.11[b]	−0.50		
$La_2@I_h$-$C_{80}(Dep_2Si)CH_2CH$(*t*-BuPh)-2B[f]	+0.13[b]	−0.53		

[a]Values obtained by DPV are in volts relative to the ferrocene/ferrocenium couple. [b]Irreversible. [c]Data from ref 5b. [d]Data from ref 17. [e]Data from ref 5c. [f]Data from ref 6.

dx.doi.org/10.1021/ja3073929 | J. Am. Chem. Soc. 2012, 134, 16033−16039

in Figure S8 (see the Supporting Information). These silylated EMFs afforded irreversible oxidation and reduction processes. The first oxidation of the silylated derivatives led to removal of the addend from the carbon cage to give $Lu_3N@I_h$-C_{80}, as observed for other silylated EMFs such as $Sc_3N@I_h$-$C_{80}(Mes_2Si)_2CH_2$.[5b] The first oxidation peak potentials of **1a** and **1b** were shifted cathodically by 340 and 180 mV, respectively, compared to those of $Lu_3N@I_h$-C_{80}. The first reduction peak potentials were also cathodically shifted by 40 mV for **1a** and 130 mV for **1b**, respectively. In addition, these cathodic shifts of the redox potentials of **1a** and **1b**, compared to those of pristine $Lu_3N@I_h$-C_{80}, are smaller than those observed for the bis-silylated EMFs $Sc_3N@I_h$-$C_{80}(Mes_2Si)_2CH_2$[5b] and $La_2@I_h$-$C_{80}(Dep_2Si)_2CH_2$.[5c] Similar weak effects on the redox potentials have been reported for the carbosilylated EMF $La_2@I_h$-$C_{80}Dep_2Si(CH_2)CH(t\text{-BuPh})$.[6] In contrast, the redox potentials of the carbene and the Bingel–Hirsch derivatives of EMFs are shifted less cathodically than **1a** and **1b**, as expected for electronically neutral carbon functional groups.[2d,13] For example, the cathodic shifts of the first oxidation potentials of carbon-bridged methano-$Lu_3N@I_h$-C_{80} derivatives are observed between 20 and 70 mV as reported by Echegoyen et al.[13b,c] These results demonstrate that introduction of silicon atoms onto the $Lu_3N@I_h$-C_{80} cage represents an effective way to raise the lowest unoccupied molecular orbital (LUMO) levels of EMF derivatives. By comparing the redox data for **1a** and **1b**, it is noteworthy that the redox potentials of the silylated EMFs depend on both the electronic properties of the exohedral functionality and the π-conjugation of the cage structures.

Theoretical Calculations. To obtain insight into the structures of the silylated products, theoretical calculations were conducted for **1a** and **1b**. The geometries of the compounds were optimized at the M06-2X[18]/6-31G(d)[19][C, H, N, Si] and LanL2DZ[20][Lu] levels as shown in Figure 8. The optimized structure of **1a** shows good agreement with the result of X-ray crystal analysis. The important calculated bond lengths are shown in Table S1, Supporting Information, for comparison with those obtained from X-ray analysis. The silylene-functionalized C–C distance is calculated as 2.261 Å, and the Si–C bond length between the addend and the I_h-C_{80} cage is almost within regular values. These results also confirm that the structure of **1a** is an open silafulleroid, which strongly supports the spectroscopic data. As shown in the X-ray structure of **1a**, the Lu1 atom points at the silylated site with an almost collinear orientation of Si1, Lu1, and N1 atoms. Therefore, we have also calculated four optimized structures, **I**–**IV**, for isomers of **1a** with varied orientations of the encapsulated Lu_3N cluster (Figure S9 in the Supporting Information). The relative energies of **I**–**IV** compared to that of **1a** are in the narrow range of 4 kcal/mol (Table S2, Supporting Information). Thus, the Lu_3N cluster can be assumed to rotate inside the cage around an axis passing along the Lu–N bond that points to the open C–C bond. In contrast, isomer **V**, in which the Lu_3N cluster is positioned on the equatorial plane viewed from the silylated site as the pole, was calculated as 18.4 kcal/mol less stable than **1a**. The calculated structure of **1b** is shown in Figure 8b. On the basis of the relative energies, these results show that **1b** is 19.2 kcal/mol less stable than **1a**. In the optimized structure of **1b**, the Lu_3N cluster is located almost coplanar with the silacyclopropane ring, and one of the Lu atoms is directed to the opposite side of the silylated C–C bond. However, no energy minimum is obtained for **1b** if the orientation of the Lu_3N cluster is reversed so that one of the Lu atoms is oriented to point at the silylated site. In this case, the silylated C–C bond is broken during the structural optimization process.

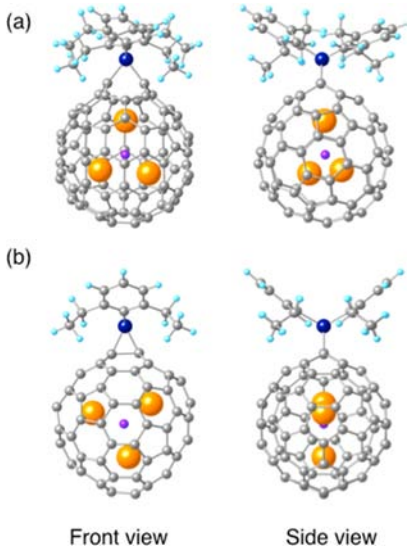

Figure 8. Optimized structures of (a) **1a** and (b) **1b**.

CONCLUSION

We have described the first example of a reaction of $Lu_3N@I_h$-C_{80} with a thermally generated silylene. A silylene adduct of $Lu_3N@I_h$-C_{80}, **1b**, is obtained as the sole product during the thermal reaction in the dark. It is particularly interesting that **1b** is transformed slowly into isomeric product **1a** under ambient light. Characterization using NMR, vis–NIR, and MS elucidated the structures of **1a** and **1b**, which were assigned respectively to [5,6]-silafulleroid and [6,6]-silacyclopropane. The structure of **1a** has been established unequivocally using single-crystal X-ray analysis. In comparison with the Prato and Bingel–Hirsch adducts of $M_3N@I_h$-C_{80} (M = Sc, Y), for which [5,6]-closed and [6,6]-open derivatives have been reported, respectively, the silylene addition is remarkable because it leads to [5,6]-open and [6,6]-closed structures. The theoretically optimized structure of **1a** verified the structural features inferred from X-ray analysis. From the calculated relative energies, **1a** is postulated to be more stable than **1b**, which might offer some clue about the photochemical transformation of **1b** into **1a**. The results of electrochemical examination indicate that, because of the electron-donating silyl groups, **1a** and **1b** are more electronegative than pristine $Lu_3N@I_h$-C_{80}. In addition to the electronic effect, exohedral functionalization affects the movement of the encapsulated cluster. Thus, the development of silylation procedures broadens the scope of functionalization of EMFs for future applications.

EXPERIMENTAL SECTION

General Procedures. All chemicals were of reagent grade, purchased from Wako Pure Chemical Industries Ltd. $Lu_3N@I_h$-C_{80} was purchased from Luna Innovations Inc. ODCB was distilled from P_2O_5 under vacuum before use. Reagents were used as purchased unless otherwise specified. HPLC was performed on an LC-908 apparatus (Japan Analytical Industry Co. Ltd.) monitored using a UV detector at 330 nm. Buckyprep (i.d. 20 mm × 250 mm) and 5NPE (i.d. 20 mm × 250 mm) columns (Nacalai Tesque Inc.) were used for

dx.doi.org/10.1021/ja3073929 | J. Am. Chem. Soc. 2012, 134, 16033–16039

preparative HPLC separation. Toluene was used as the eluent for HPLC. The ^{1}H, ^{13}C, and ^{29}Si NMR measurements were conducted on spectrometers (AVANCE 500 and 600, Bruker Analytik GmbH) with a CryoProbe system (Bruker Biospin K.K.) in 1,1,2,2-tetrachloroethane-d_2. The outer standard reference was tetramethylsilane (TMS) for ^{29}Si NMR. MALDI-TOF mass experiments were recorded (Biflex III, Bruker) with 1,1,4,4-tetraphenyl-1,3-butadiene (TPB) as the matrix in both positive and negative ion modes. Absorption spectra were measured using a UV spectrophotometer (UV-3150, Shimadzu Corp.). Cyclic voltammograms and differential pulse voltammograms were recorded on an electrochemical analyzer (BAS CV50W, BAS Inc.). The reference electrode was a saturated calomel reference electrode (SCE). The glassy carbon electrode was used as the working electrode, and a platinum wire was used as the counter electrode. All potentials are referenced to the ferrocene/ferrocenium couple (Fc/Fc^{+}) as the standard. $(n\text{-Bu})_4NPF_6$ (0.1 M) in ODCB was used as the supporting electrolyte solution. The cyclic voltammograms were recorded using a scan rate of 100 mV/s. The differential pulse voltammograms were obtained using a pulse amplitude of 50 mV, a pulse width of 50 ms, a pulse period of 200 ms, and a scan rate of 50 mV/s.

Thermal Reaction of $Lu_3N@I_h$-C_{80} with 2. An ODCB solution (20 mL) of $Lu_3N@I_h$-C_{80} (2.0 mg, 1.3×10^{-6} mol) and **2** (13.7 mg, 3.4×10^{-5} mol) was degassed using freeze–pump–thaw cycles under reduced pressure in a Pyrex tube. The solution was heated at 180 °C for 23 min under an argon atmosphere in the dark. When the reaction was finished, **1b** was detected as the sole product. Subsequently, slow photochemical transformation of **1b** into **1a** was observed under ambient light. The reaction mixture was separated by preparative HPLC with Buckyprep and 5NPE columns to isolate **1a** and **1b**, respectively, in 20% and 33% yields.

*Data for **1a**:* red solid; ^{1}H NMR (500 MHz, $C_2D_2Cl_4$, 293 K) δ 7.47 (t, J = 8 Hz, 1H), 7.42 (t, J = 8 Hz, 1H), 7.30 (d, J = 7.5 Hz, 2H), 7.21 (d, J = 8 Hz, 2H), 3.88–3.81 (m, 2H), 3.67–3.55 (m, 4H), 3.29–3.21 (m, 2H), 1.46 (t, J = 7.5 Hz, 6H), 1.43 (t, J = 7.5 Hz, 6H); ^{13}C NMR (125 MHz, $C_2D_2Cl_4$, 293 K) δ 151.24 (2C, *o*-Ar), 151.10 (2C, *o*-Ar), 150.86 (2C), 148.28 (2C), 148.04 (1C), 147.76 (2C), 146.70 (2C), 145.82 (2C), 145.51 (1C), 145.23 (2C), 145.12 (2C), 144.92 (2C), 143.58 (1C), 143.43 (4C), 143.30 (2C), 143.00 (2C), 142.82 (2C), 142.63 (2C), 142.36 (2C), 142.24 (2C), 142.16 (2C), 141.69 (2C), 141.64 (2C), 141.55 (2C), 140.92 (2C), 140.63 (2C), 140.51 (2C), 140.26 (2C), 139.93 (2C), 139.63 (1C), 139.50 (1C), 139.25 (2C), 139.06 (2C), 138.31 (1C), 138.02 (2C), 136.85 (2C), 136.32 (2C), 136.06 (2C), 135.74 (2C), 133.11 (1C), 132.15 (1C), 131.79 (1C, *p*-Ar), 131.57 (1C, *p*-Ar), 126.80 (2C, *m*-Ar), 126.75 (2C, *m*-Ar), 125.01 (1C), 124.85 (1C), 123.80 (2C), 122.72 (2C), 110.82 (2C), 72.80 (2C, C_{80}Si), 31.42 (2C, CH_2), 30.73 (2C, CH_2), 16.16 (2C, CH_3), 15.76 (2C, CH_3); ^{29}Si NMR (119.4 MHz, $C_2D_2Cl_4$, 298 K) δ −57.24; MALDI-TOF MS (TPB) m/z 1793 ($[M]^{+}$), 1499 ($[M - C_{20}H_{26}Si]^{+}$).

*Data for **1b**:* red solid; ^{1}H NMR (500 MHz, $C_2D_2Cl_4$, 293 K) δ 7.50 (t, 2H, J = 7.5 Hz), 7.31 (br, 2H), 7.25 (br, 2H), 3.48 (br, 4H), 3.40 (br, 2H), 3.31 (br, 2H), 1.43 (br, 6H), 1.30 (br, 6H); ^{13}C NMR (125 MHz, $C_2D_2Cl_4$, 293 K) δ 152.22 (2C), 151.18 (2C, *o*-Ar), 151.00 (2C, *o*-Ar), 150.05 (2C), 148.34 (2C), 146.76 (2C), 146.40 (2C), 146.05 (1C), 145.52 (2C), 145.40 (2C), 145.10 (2C), 144.74 (2C), 144.47 (2C), 143.97 (2C), 143.92 (2C), 143.66 (2C), 143.02 (2C), 142.99 (4C), 142.83 (2C), 142.72 (1C), 142.10 (2C), 141.90 (2C), 141.78 (2C), 141.31 (1C), 141.02 (2C), 140.86 (2C), 140.51 (2C), 140.44 (2C), 140.12 (2C), 139.60 (2C), 138.86 (2C), 138.29 (1C), 137.64 (2C), 135.43 (1C), 135.35 (2C), 135.23 (2C), 134.77 (2C), 134.05 (3C), 132.01 (2C, *p*-Ar), 127.87 (2C), 126.84 (2C, *m*-Ar), 126.70 (2C, *m*-Ar), 126.54 (2C), 125.81 (2C), 124.91 (2C), 122.33 (2C), 85.14 (1C, C_{80}Si), 77.17 (1C, C_{80}Si), 31.34 (2C, CH_2), 31.13 (2C, CH_2), 15.86 (2C, CH_3), 15.44 (2C, CH_3); ^{29}Si NMR (119.4 MHz, $C_2D_2Cl_4$, 298 K) δ −53.12; vis–NIR (CS_2) λ_{max} 698 nm; MALDI-TOF MS (TPB) m/z 1793 ($[M]^{+}$), 1499 ($[M - C_{20}H_{26}Si]^{+}$).

X-ray Crystallography of 1a. Crystals of **1a** were obtained using the liquid–liquid bilayer diffusion method of an CS_2/ODCB = 1/1 solution of **1a** using hexane as a poor solvent at 0 °C. Single-crystal X-ray diffraction data of **1a** were collected on a Bruker AXS machine equipped with an Apex II charge-coupled device (CCD) detector and a liquid nitrogen low-temperature apparatus providing a constant temperature at 90 K.

*Crystal data for **1a**, $Lu_3N@I_h$-C_{80}-SiDep$_2$·CS_2:* $C_{101}H_{26}Lu_3NS_2Si$, M_r = 1870.35, red platelet, 0.18 × 0.16 × 0.04 mm, orthorhombic, *Pccn* (No. 56), a = 10.9576(10) Å, b = 17.2860(15) Å, c = 28.760(2) Å, V = 5447.5(8) Å^3, Z = 4, λ = 0.71073 Å, μ(Mo Kα) = 5.564 mm^{-1}, θ_{max} = 28.69°, D_{calcd} = 2.281 g/cm^3, T = 90 K, 34 063 measured reflections, 6916 independent reflections, 473 refined parameters, R1 = 0.1221, wR2 = 0.2339 for all data, GOF = 1.278 for all data, R1 = 0.1043 for 6916 independent reflections [$I > 2.0\sigma(I)$] with 473 parameter and 776 restraints.

Computational Method. Theoretical calculations were conducted for **1a** and **1b**. The geometries of the compounds were optimized at the M06-2X[18]/6-31G(d)[19][C, H, N, Si] and LanL2DZ[20][Lu] levels using the Gaussian 09[21] program.

■ ASSOCIATED CONTENT

Supporting Information

X-ray crystallographic data for **1a** in CIF format, spectroscopic data for **1a** and **1b**, synthesis of **2**, and complete lists of authors for refs 2c–2e, 3b, 4b, 5a–5c, 8a–8c, 8f, 12, 14b, 15b, and 21. This material is available free of charge via the Internet at http://pubs.acs.org .

■ AUTHOR INFORMATION

Corresponding Author

akasaka@tara.tsukuba.ac.jp

Notes

The authors declare no competing financial interest.

■ ACKNOWLEDGMENTS

This work was supported by a Grant-in-Aid for Scientific Research on Innovative Areas (20108001, "pi-Space"), Grants-in-Aid for Scientific Research (A) (20245006) and (B) (24350019), The Next Generation Super Computing Project (Nanoscience Project), the Nanotechnology Support Project, Grants-in-Aid for Scientific Research on Priority Area (20036008 and 20038007), Specially Promoted Research (Grant 22000009) from the Ministry of Education, Culture, Sports, Science, and Technology of Japan, and The Strategic Japanese–Spanish Cooperative Program funded by JST and MICINN.

■ REFERENCES

(1) (a) *Endofullerenes: A New Family of Carbon Clusters*; Akasaka, T., Nagase, S., Eds.; Kluwer: Dordrecht, The Netherlands, 2002. (b) Martín, N. *Chem. Commun.* **2006**, 2093–2104. (c) Dunsch, L.; Yang, S. *Phys. Chem. Chem. Phys.* **2007**, *9*, 3067–3081. (d) Dunsch, L.; Yang, S. *Small* **2007**, *3*, 1298–1320. (e) Chaur, M. N.; Melin, F.; Ortiz, A. L.; Echegoyen, L. *Angew. Chem., Int. Ed.* **2009**, *48*, 7514–7538. (f) Tan, Y. Z.; Xie, S. Y.; Huang, R. B.; Zheng, L. S. *Nat. Chem.* **2009**, *1*, 450–460. (g) Yamada, M.; Akasaka, T.; Nagase, S. *Acc. Chem. Res.* **2010**, *43*, 92–102. (h) *Chemistry of Nanocarbons*; Akasaka, T., Wudl, F., Nagase, S., Eds.; Wiley: Chichester, U.K., 2010.

(2) (a) Kobayashi, S.; Mori, S.; Iida, S.; Ando, H.; Takenobu, T.; Taguchi, Y.; Fujiwara, A.; Taninaka, A.; Shinohara, H.; Iwasa, Y. *J. Am. Chem. Soc.* **2003**, *125*, 8116–8117. (b) Yasutake, Y.; Shi, Z.; Okazaki, T.; Shinohara, H.; Majima, Y. *Nano Lett.* **2005**, *5*, 1057–1060. (c) Tsuchiya, T.; et al. *J. Am. Chem. Soc.* **2008**, *130*, 450–451. (d) Ross, R. B.; et al. *Nat. Mater.* **2009**, *8*, 208–212. (e) Sato, S.; et al. *J. Am. Chem. Soc.* **2011**, *133*, 2766–2771.

(3) (a) Cagle, D. W.; Kennel, S. J.; Mirzadeh, S.; Alford, J. M.; Wilson, L. J. *Proc. Natl. Acad. Sci. U.S.A.* **1999**, *96*, 5182–5187. (b) Fatouros, P. P.; et al. *Radiology* **2006**, *240*, 756–764.

(4) (a) Wakahara, T.; Kako, M.; Maeda, Y.; Akasaka, T.; Kobayashi, K.; Nagase, S. *Curr. Org. Chem.* **2003**, *7*, 927−943. (b) Nagatsuka, J.; et al. *J. Am. Chem. Soc.* **2010**, *132*, 12106−12120 and references cited therein.
(5) (a) Yamada, M.; et al. *J. Am. Chem. Soc.* **2005**, *127*, 14570−14571. (b) Wakahara, T.; et al. *J. Am. Chem. Soc.* **2006**, *128*, 9919−9925. (c) Wakahara, T.; et al. *Chem. Commun.* **2007**, 2680−2682. (d) Yamada, M.; Wakahara, T.; Tsuchiya, T.; Maeda, Y.; Kako, M.; Akasaka, T.; Yoza, K.; Horn, E.; Mizorogi, N.; Nagase, S. *Chem. Commun.* **2008**, 558−560.
(6) Yamada, M.; Minowa, M.; Sato, S.; Kako, M.; Slanina, Z.; Mizorogi, N.; Tsuchiya, T.; Maeda, Y.; Nagase, S.; Akasaka, T. *J. Am. Chem. Soc.* **2010**, *132*, 17953−17960.
(7) Gaspar, P. P.; West, R. In *The Chemistry of Organosilicon Compounds*; Patai, S., Rappoport, Z., Eds.; Wiley: Chichester, U.K., 1998; Vol. 2, Part 3, Chapter 43, p 2463.
(8) (a) Maeda, Y.; et al. *J. Am. Chem. Soc.* **2004**, *126*, 6858−6859. (b) Iiduka, Y.; et al. *J. Am. Chem. Soc.* **2005**, *127*, 12500−12501. (c) Iiduka, Y.; et al. *Angew. Chem., Int. Ed.* **2007**, *46*, 5562−5564. (d) Cao, B.; Nikawa, H.; Nakahodo, T.; Tsuchiya, T.; Maeda, Y.; Akasaka, T.; Sawa, H.; Slanina, Z.; Mizorogi, N.; Nagase, S. *J. Am. Chem. Soc.* **2008**, *130*, 983−989. (e) Yamada, M.; Someya, C.; Wakahara, T.; Tsuchiya, T.; Maeda, Y.; Akasaka, T.; Yoza, K.; Horn, E.; Mizorogi, N.; Nagase, S. *J. Am. Chem. Soc.* **2008**, *130*, 1171−1176. (f) Ishitsuka, M. O.; et al. *J. Am. Chem. Soc.* **2011**, *133*, 7128−7134. (g) Liu, T.-X.; Wei, T.; Zhu, S.-E.; Wang, G.-W.; Jiao, M.; Yang, S.; Bowles, F. L.; Olmstead, M. M.; Balch, A. L. *J. Am. Chem. Soc.* **2012**, *134*, 11956−11959.
(9) (a) Hirsch, A. *The Chemistry of Fullerenes*; Thieme: Stuttgart, Germany, 1994. (b) Taylor, R. *The Chemistry of Fullerenes*; World Scientific: Singapore, 1995. (c) Hirsch, A. *Synthesis* **1995**, 895−913. (d) Averdung, J.; Torres-Garcia, G.; Luftmann, H.; Schlachter, I.; Mattay, J. *Fullerene Sci. Technol.* **1996**, *4*, 633−654. (e) Langa, F.; Nierengarten, J. F. *Fullerenes: Principles and Applications*; RSC Publishing: London, 2007.
(10) (a) Akasaka, T.; Ando, W.; Kobayashi, K.; Nagase, S. *J. Am. Chem. Soc.* **1993**, *115*, 1605−1606. (b) Akasaka, T.; Mitsuhida, E.; Ando, W.; Kobayashi, K.; Nagase, S. *J. Chem. Soc., Chem. Commun.* **1995**, 1529−1530.
(11) (a) Stevenson, S.; Lee, H. M.; Olmstead, M. M.; Kozikowski, C.; Stevenson, P.; Balch, A. L. *Chem.—Eur. J.* **2002**, *8*, 4528−4535. (b) Iezzi, E. B.; Duchamp, J. C.; Fletcher, K. R.; Glass, T. E.; Dorn, H. C. *Nano Lett.* **2002**, *2*, 1187−1190.
(12) Shu, C. Y.; et al. *J. Am. Chem. Soc.* **2008**, *130*, 17755−17760.
(13) (a) Shu, C. Y.; Cai, T.; Xu, L. S.; Zuo, T. M.; Reid, J.; Harich, K.; Dorn, H. C.; Gibson, H. W. *J. Am. Chem. Soc.* **2007**, *129*, 15710−15717. (b) Pinzón, J. R.; Zuo, T. M.; Echegoyen, L. *Chem.—Eur. J.* **2010**, *16*, 4864−4869. (c) Li, F.-F.; Rodríguez-Fortea, A.; Poblet, J. M.; Echegoyen, L. *J. Am. Chem. Soc.* **2011**, *133*, 2760−2765.
(14) (a) Lukoyanova, O.; Cardona, C. M.; Rivera, J.; Lugo-Morales, L. Z.; Chancellor, C. J.; Olmstead, M. M.; Rodríguez-Fortea, A.; Poblet, J. M.; Balch, A. L.; Echegoyen, L. *J. Am. Chem. Soc.* **2007**, *129*, 10423−10430. (b) Shu, C.; et al. *Org. Lett.* **2009**, *11*, 1753−1756.
(15) (a) Yamada, M.; Wakahara, T.; Nakahodo, T.; Tsuchiya, T.; Maeda, Y.; Akasaka, T.; Yoza, K.; Horn, E.; Mizorogi, N.; Nagase, S. *J. Am. Chem. Soc.* **2006**, *128*, 1402−1403. (b) Cai, T.; et al. *J. Am. Chem. Soc.* **2006**, *128*, 6486−6492.
(16) Yamada, M.; Minowa, M.; Sato, S.; Slanina, Z.; Tsuchiya, T.; Maeda, Y.; Nagase, S.; Akasaka, T. *J. Am. Chem. Soc.* **2011**, *133*, 3796−3799.
(17) Suzuki, T.; Maruyama, Y.; Kato, T.; Kikuchi, K.; Nakao, Y.; Achiba, Y.; Kobayashi, K.; Nagase, S. *Angew. Chem., Int. Ed. Engl.* **1995**, *34*, 1094−1096.
(18) (a) Zhao, Y.; Truhlar, D. G. *Theor. Chem. Acc.* **2008**, *120*, 215−241. (b) Zhao, Y.; Truhlar, D. G. *J. Chem. Phys.* **2006**, *125*, 194101/1−194101/18. (c) Zhao, Y.; Truhlar, D. G. *J. Phys. Chem. A* **2005**, *109*, 5656−5667.
(19) Hehre, W. J.; Ditchfield, R.; Pople, J. A. *J. Chem. Phys.* **1972**, *56*, 2257−2261.
(20) Hay, P. J.; Wadt, W. R. *J. Chem. Phys.* **1985**, *82*, 299−310.
(21) Frisch, M. J.; et al. *Gaussian 09, Revision C.01*; Gaussian, Inc.: Wallingford, CT, 2010.